

**Limits on the validity of infinite length assumptions for
modelling shallow landslides**

Journal:	<i>Earth Surface Processes and Landforms</i>
Manuscript ID:	ESP-11-0234.R1
Wiley - Manuscript type:	Paper
Date Submitted by the Author:	14-Dec-2011
Complete List of Authors:	Milledge, David; Durham University, Institute of Hazard Risk and Resilience; Durham University, Department of Geography Griffiths, D; Colorado School of Mines, Division of Engineering Lane, Stuart; Université de Lausanne, Institut de géographie Warburton, Jeff; Durham University, Department of Geography
Keywords:	infinite slope length, stability model, shallow landslide, finite element method, benchmark

SCHOLARONE™
Manuscripts

1 Limits on the validity of infinite length assumptions for 2 modelling shallow landslides

3 Abstract

4 The infinite slope method is widely used as the geotechnical component of geomorphic and
5 landscape evolution models. Its assumption that shallow landslides are infinitely long is usually
6 considered valid for natural landslides on the basis that they are generally long relative to their depth.
7 However, this is rarely justified because we lack a clear definition of the critical length / depth ratio
8 below which edge effects become important and length dependence appears. Here we benchmark
9 infinite slope predictions across the range of possible slope properties found on natural slopes to
10 establish the critical length at which infinite slope stability predictions fall within 5 and 10% of those
11 estimated by a finite element method. We find that infinite slope stability predictions always
12 converge to within 5% of the finite element benchmarks at a critical length / depth ratio of 25.
13 However, they can converge at much lower ratios depending on slope properties, particularly the
14 proportions of cohesive versus frictional soil strength so that critical length depth ratios are smaller
15 for low cohesion soils. As a result the infinite length assumption within the infinite slope method is
16 valid for catchment scale models when their grid resolution is coarse (e.g. >25 m). However, it may
17 also be important when their grid resolution is much finer, because spatial organisation in the
18 predicted pore water pressure field reduces the probability of short landslides and minimises the risk
19 that predicted landslides will have length / depth ratio's less than 25.

20
21 Keywords: infinite slope length, stability model, shallow landslide, finite element method,
22 benchmark.

23

24 Background

1
2
3 25 Shallow landslides are important agents of erosion and sources of sediment in terrestrial
4
5 26 environments and need to be represented in geomorphic (e.g. Montgomery and Dietrich, 1994;
6
7 27 Bathurst *et al.*, 2005; Reid *et al.*, 2007) and landscape evolution models (e.g. Tucker and Bras,
8
9 28 1998). However, a full stability analysis at every potential landslide site is not feasible; therefore
10
11 29 much work has focussed on trying to develop simple physically based methods to identify shallow
12
13 30 landslide risk comparatively across the landscape (e.g. Montgomery and Dietrich, 1994; Baum *et al.*,
14
15 31 2008).
16
17
18
19
20

21 33 The infinite slope method (Taylor, 1948; Haefeli, 1948; Skempton and DeLory, 1957) is widely used
22
23 34 as the geotechnical component of these geomorphic and landscape evolution models where it is
24
25 35 generally combined with a hydrological model to predict pore water pressure and hence failure
26
27 36 probability. Much attention in developing these models has been focussed on different approaches to
28
29 37 predicting the spatial pore water pressure patterns (Montgomery and Dietrich, 1994; Burton and
30
31 38 Bathurst, 1995; Wu and Sidle, 1995; Reid *et al.*, 2007; Simoni *et al.*, 2008; Baum *et al.*, 2008).
32
33 39 However, much less attention has been given to the geotechnical component. This is partly because
34
35 40 the assumptions behind the infinite slope method, particularly of infinite width and length (Skempton
36
37 41 and DeLory, 1957), are considered valid for many natural landslides, which have relatively high
38
39 42 length (L) / depth (H) ratios (Haneberg, 2004). Furthermore, attempts to account for the influence of
40
41 43 the landslide margins on the balance of forces requires additional assumptions to be made about the
42
43 44 location, orientation, and magnitude of the forces involved.
44
45
46
47
48
49

50 46 The argument that the infinite slope method is suitable for shallow landslides because they have high
51
52 47 length / depth (L/H) ratios is frequently stated but rarely justified (Wu and Sidle, 1995; Iverson,
53
54 48 2000; Crosta and Frattini, 2002; Casadei *et al.*, 2003; Haneberg, 2004; Bathurst *et al.*, 2005; Ray *et*
55
56 49 *al.*, 2010). Most natural landslides are shallow, Figure 1 shows two example inventories where L/H
57
58 50 ratios exceed 7 for >90% of landslides (Gabet and Dunne, 2002; Warburton *et al.*, 2008), while the
59
60

1 51 scaling analysis of Larsen *et al.* (2010) suggests L/H ratio increases with length ($L/H = 12.5 L^{0.16}$)
2 52 and exceeds 18 even for very small landslides ($L < 4$ m). However, we cannot assume that the infinite
3 53 slope method is suitable for these landslides without more rigorous testing. This requires an
4 54 assessment of the L/H ratio of the predicted or observed landslides relative to the L/H ratio at which
5 55 infinite slope assumptions break down.
6
7
8
9

10 56

11
12
13 57 <Figure 1 near here>
14
15

16 58

17
18 59 Recent work by Griffiths *et al.* (2011) has begun to address this by benchmarking infinite slope
19 60 predictions against those from a finite element (FE) continuum mechanics method. The rationale for
20 61 this is that the FE predictions can be assumed as a benchmark for the stability of a given slope. This
21 62 is reasonable since they have been shown to be reliable and robust for assessing the factor of safety
22 63 of slopes across a range of scenarios (Griffiths and Lane, 1999). They perform at least as well as
23 64 limit equilibrium methods for known parametric tests (Hammah *et al.*, 2005) but are far more
24 65 flexible, not requiring assumptions about: the shape or location of the failure surface, nor the inter-
25 66 slice forces (Griffiths and Lane, 1999). On this basis, infinite slope stability predictions can then be
26 67 tested against the FE predictions for different slope lengths.
27
28
29
30
31
32
33
34
35
36
37

38 68

39
40 69 Griffiths *et al.* (2011) find that the FE predictions converge on those from the infinite slope method
41 70 at L/H ratios of around 16 and suggest that, in general, the infinite slope method is suitable for $L/H >$
42 71 16. However they show that for slopes with shorter L/H ratios the infinite slope method predictions
43 72 become increasingly different to the benchmark as L/H decreases. At an L/H ratio of two, the infinite
44 73 slope method can predict that a slope is less than half as stable as the FE method predicts for the
45 74 same slope. They attribute this difference to error in the infinite slope method resulting from the
46 75 violation of its infinite length assumption. This has potentially significant implications for the
47 76 appropriateness of the infinite slope method for geomorphic modelling. Such models often rely on
48 77 cell-by-cell calculations of infinite-slope stability with resolutions ranging from a few to tens of
49 78 meters. The often implicit assumption in applying these models is that the grid cells are adequately
50
51
52
53
54
55
56
57
58
59
60

79 long relative to the landslide failure plane depth so that factors of safety calculated with an infinite
80 slope approach are reasonably free of error. If the findings of Griffiths *et al.* (2011) hold across the
81 full range of natural slope conditions then this assumption would be valid for models with grid cells
82 longer than 16 times the assumed failure plane depth but could introduce error at finer resolutions. In
83 this paper we extend some of the initial conclusions from Griffiths *et al.* (2011) to establish the
84 generality of their findings; then assess the implications of these findings for stability analysis within
85 geomorphology and landscape evolution models.

86

87 ***The Infinite Slope Method***

88 The most common geotechnical measure of slope stability is the factor of safety (*FoS*) the ratio of
89 shear strength of the soil (*s*) to the shear stress (τ) required for equilibrium.

90

Equation 1

$$91 \quad FoS = \frac{s}{\tau}$$

92 A slope is considered to be just stable when the stresses and strengths are equal and the *FoS* is equal
93 to one and to fail for $FoS < 1$. The factor of safety can be calculated using a range of approaches,
94 including the one dimensional infinite slope method, and more sophisticated limit equilibrium and
95 continuum mechanics methods in two and three-dimensions. More sophisticated methods allow
96 improved representation of the failure geometry. However, they require fine scale discretisation of
97 the slope, phreatic surface and failure plane geometries and generally need to be solved iteratively.
98 These data and computational requirements limit their applicability at the catchment scale where
99 analysis almost invariably involves the simpler one-dimensional infinite slope method.

100

101 <Figure 2 near here>

102

103 The Infinite Slope (IS) method (Taylor, 1948; Haefeli, 1948; Skempton and DeLory, 1957) makes
104 two key assumptions: 1) that sliding occurs along a pre-defined plane parallel to the face of the
105 slope; and 2) that the sliding block is infinitely long and wide so that stresses are the same on the two

106 planes perpendicular to the slope (e.g. stresses A-A' = stresses B-B' in Figure 2). These stresses are
 107 collinear, equal in magnitude and opposite in direction. Therefore they exactly balance each other
 108 and can be ignored. The equilibrium equations are derived using a rectangular block (e.g. A-B-B'-
 109 A'). All the stresses perpendicular (σ) and parallel (τ) to the failure plane are summed to give:

110 **Equation 2**

$$111 \tau = W \sin \beta = \gamma_s H \cos \beta \sin \beta$$

112 **Equation 3**

$$113 \sigma = \cos \beta W = \cos^2 \beta \gamma_s H$$

114 where: β is the block's slope [-]; W is the weight of the block [kN]; σ is the normal stress on the slip
 115 plane [kPa]; γ_s is the soil unit weight [kN m^{-3}]; and H is the vertical depth to the shear plane [m].

116 Assuming steady seepage parallel to the slope at a depth of H_w above the failure plane [m], we can
 117 account for the effect of pore water pressure (u) [kPa] on normal stress to calculate the effective
 118 normal stress using:

119 **Equation 4**

$$120 \sigma - u = \cos^2 \beta (\gamma_s (H - H_w) + (\gamma_s - \gamma_w) H_w) = \cos^2 \beta H (\gamma_s - \gamma_w m)$$

121 where: γ_w is the water unit weight [kN m^{-3}]; and m is the normalised free surface height [-] defined as
 122 $m = H_w/H$; $m=1$ for fully saturated flow with the phreatic surface at the ground surface, and $m=0$ for
 123 "dry" cases where the phreatic surface is below the failure plane and does not affect the stability.

124 Shear strength (s) [kPa] for effective stresses is expressed by the Mohr–Coulomb equation as:

125 **Equation 5**

$$126 s = c' + (\sigma - u) \tan \varphi'$$

127 where: c' is the effective soil cohesion [kPa]; and φ' is the effective friction angle [-]. Substituting
 128 Equation 2, Equation 3 and Equation 5 into Equation 1 to calculate the factor of safety (FoS) [-]
 129 gives:

130 **Equation 6**

$$131 FoS = \frac{c' + \cos^2 \beta H (\gamma_s - \gamma_w m) \tan \varphi'}{\gamma_s H \cos \beta \sin \beta}$$

132 This provides a very simple one-dimensional balance of forces equation for slope stability that can
 133 be easily applied within a spatial model for landslides since the stability of each element can be
 134 calculated independent of its neighbours.

135

1
2
3 136 However, its validity and predictive ability is defined by the extent to which its assumptions are met.
4
5 137 Griffiths *et al.*, (2011) have suggested that the infinite length assumption is reasonable for L/H ratios
6
7 138 greater than 16. However, before we can use this as a critical L/H ratio when assessing the suitability
8
9 139 of the infinite slope method for catchment modelling we need to know: 1) how general this result is
10
11 140 under the range of plausible conditions found in natural landscapes; and 2) which slope properties, if
12
13 141 any, influence the magnitude of the critical L/H ratio.
14

142

143 **Method**

144 ***Parameter exploration***

145 To address these questions we explored the influence of L/H ratio on the accuracy of the infinite
146 slope method by benchmarking it against the same finite element method as Griffiths *et al.* (2011).
147 To establish the generality of the relationships we varied all the other parameters within the infinite
148 slope equation (Equation 6, cohesion, friction angle, soil depth, normalised free surface height, soil
149 unit weight and slope angle). We varied these parameters across their reasonable ranges (Table 1)
150 and assessed the impact of these variations on the critical L/H ratio (L/H_{crit}) at which the infinite
151 slope predictions converged with those from the finite element method.

152

153 Our experimental design for the parameter exploration had two components. First, we used a
154 systematic parameter exploration to test the method's performance for a set of extreme parameter
155 combinations at the limits of the parameter space. The parameters and their limits are listed in Table
156 1. In each case we used the FE method to predict FoS at L/H ratios of: 4, 8, 12, 16, 24 and 48. These
157 ratios were chosen after initial tests in order to sample most densely in the region of expected
158 convergence for the two methods but with some samples at longer L/H ratios to ensure that any
159 extreme responses were captured. We then compared the FE and IS predictions, standardising the
160 results by expressing the difference between predictions as a percentage of the FE FoS . The
161 systematic parameter exploration is useful in illustrating the form of the FoS difference curves across

162 the reasonable range of slope properties. However, it is difficult to interpret in terms of the influence
163 of individual parameters on the L/H_{crit} value because: 1) it only shows results for the extreme limits
164 to the slope properties; and 2) the parameter combinations are difficult to differentiate.

165

166 Second, we addressed the limitations above using a random parameter exploration. Here, we applied
167 a Monte Carlo approach, sampling each of the six infinite slope parameters randomly and assuming a
168 uniform distribution across the range defined in Table 1. Although some of the parameters in the IS
169 method tend to co-vary (e.g. ϕ' and c') we sampled from uniform distributions and avoided *a priori*
170 assumptions about their covariance because we were interested in the sensitivity of the method to the
171 full range of possible conditions and so needed broad and uniform coverage of the parameter space.
172 This generated 5000 synthetic slopes with random slope geometry and material properties. For each
173 of these we then calculated stability using the FE and IS methods for the same set of L/H ratios used
174 in the first parameter exploration. Again the error in the IS predictions was expressed as a percentage
175 of the FE FoS . The L/H_{crit} at which the FE method converged to within 5% and 10% of the IS
176 predictions was recorded. These critical L/H ratios could then be plotted against each parameter to
177 show the influence of that parameter on L/H_{crit} . The systematic tests (from the first step) could be
178 used to ensure that the extremes of the parameter ranges have been sampled and to ensure confidence
179 in our assertion about the maximum L/H ratio required to satisfy the infinite slope assumptions. Both
180 the systematic and Monte Carlo explorations involved modifying the parameters in combination (as
181 opposed to one at a time) to account for interaction effects between parameters.

182

183 <Table 1 near here>

184

185 **Finite Element method**

186 To benchmark the infinite slope predictions for slopes of a defined length, we compare them with a
187 finite element method developed by Griffiths and Lane (1999) and modified by Griffiths *et al.*
188 (2011) to make it suitable for landslides on long slopes with very high L/H ratios. The method has
189 been validated against the infinite slope method for scenarios where the FE domain simulates infinite

190 length conditions (Griffiths *et al.*, 2011, Sections 4 and 5). The model performs 2D plane strain
191 analysis of elastic-perfectly plastic soils with a Mohr-Coulomb failure criterion using 8-node
192 quadrilateral elements with reduced integration (4 Gauss-points per element) in the gravity loads
193 generation, the stiffness matrix generation and the stress redistribution phases of the algorithm. The
194 soil is initially assumed to be elastic and the model generates normal and shear stresses at all Gauss-
195 points within the mesh. These stresses are then compared with the Mohr-Coulomb failure criterion.
196 If the stresses at a particular Gauss-point lie within the Mohr-Coulomb failure envelope then that
197 location is assumed to remain elastic. If the stresses lie on or outside the failure envelope, then that
198 location is assumed to be yielding. Yield stresses are redistributed throughout the mesh using the
199 visco-plastic algorithm (Perzyna 1966, Zienkiewicz *et al.* 1975). Overall shear failure occurs when a
200 sufficient number of Gauss-points have yielded to allow a mechanism to develop. The factor of
201 safety is defined as the ratio of the average shear strength of the soil to the average shear stress
202 developed along the critical failure surface and is calculated using the shear strength reduction
203 technique (Zienkiewicz *et al.*, 1975).

204
205 The domain geometry and boundary conditions are designed to represent slopes of a finite length.
206 They should be simple enough to isolate the effect of length on stability but representative so that we
207 can be confident that our conclusions apply to natural slopes. We use a mesh of 8-noded
208 quadrilateral elements (shown in Figure 3). The mesh consists of horizontal sections to the left and
209 right, and a long sloping central section. The base of the mesh is fully fixed and the extreme vertical
210 boundaries to the left and right allow vertical movement only. This simple representation of a finite
211 slope, with a sloping section between two horizontal sections, is common in slope stability modelling
212 (Chugh, 2003). The boundary conditions on the base are exactly the same as in the IS method in that
213 shearing can occur at the base of the soil layer. We chose fixed rather than periodic vertical
214 boundaries since we are interested in the IS method's ability to represent finite slopes. We added
215 horizontal sections 4 times the domain depth and allowed vertical movement on the vertical
216 boundaries to minimize edge effects. The size of real landslides is defined not only by a slope's
217 geometry but also its pore water pressure and material properties, which vary across the slope. This

1 218 variability might be responsible for defining the unstable part of a slope but cannot be represented
2 219 within the IS method. The simplest way of creating a zone of decreased stability between two more
3 220 stable zones is to change the domain geometry at the head and toe. In this respect we are changing
4 221 the geometry to create more stable regions and ensure that the failure is a finite (defined) length. We
5 222 tested end sections inclined at a range of angles but found that for sloping end sections the failure
6 223 can expand to fill the full domain. This increases the influence of the vertical boundary conditions
7 224 and alters the geometry of the failure plane so that it is no longer consistent with the IS method. We
8 225 chose horizontal sections for consistency and simplicity. This represents both the specific case of a
9 226 finite slope with uniform material properties and horizontal sections above and below it and the more
10 227 general case of a slope with more stable zones above and below it. Our tests using a sloping end
11 228 sections showed that where the failure was limited to the sloping section change in inclination of the
12 229 end sections lead to only minor changes in predicted stability.

13 230

14 231 <Figure 3 near here>

15 232

16 233 We represent the slope geometry and soil properties using the six parameters shown in Table 1 with
17 234 elastic parameters Young's modulus and Poisson's ratio, which are needed by the displacement-
18 235 based FE formulation to introduce stresses into the model. These elastic parameters have been shown
19 236 to have little influence on stability predictions (Hammah *et al.*, 2005) and are held constant
20 237 throughout the study at nominal values of 10^5 kPa and 0.3 respectively.

21 238

22 239 The FE model has one further soil parameter, the dilation angle, which affects the volume change of
23 240 the soil during yielding. It is well known that the actual volume change exhibited by a soil during
24 241 yielding is quite variable. For example a medium dense material during shearing might initially
25 242 exhibit some volume decrease ($\psi < 0$) followed by a dilative phase ($\psi > 0$), leading eventually to
26 243 yield under constant volume conditions ($\psi = 0$). Clearly this type of detailed volumetric modelling is
27 244 beyond the scope of the elastic-perfectly plastic models used in this study where a constant dilation
28 245 angle is implied. The question then arises as to what value of ψ to use. If $\psi = \phi$ then the plasticity

246 flow rule is 'associated' and direct comparisons with theorems from classical plasticity can be made.
247 In spite of this potential advantage, it is also well known that associated flow rules with frictional
248 soil models predict far greater dilation than is ever observed in reality. This in turn leads to increased
249 failure load prediction, especially in confined problems such as bearing capacity (e.g. Griffiths
250 1982). Slope stability analysis, especially with long slopes, is relatively unconfined, thus the choice
251 of dilation angle is less important (Griffiths and Marquez, 2007). As the main objective of the
252 current study is the accurate prediction of slope factors of safety, a compromise value of $\psi = 0$,
253 corresponding to a non-associated flow rule with zero volume change during yield, has been used
254 throughout this paper. This value of ψ enables the model to give reliable factors of safety and a
255 reasonable indication of the location and shape of the potential failure surfaces.

256

257 **Results**

258 ***Systematic parameter exploration***

259 For a given slope geometry and set of material properties Figure 4a shows that the FoS predicted by
260 the FE method at a L/H ratio of 2 is very high, almost double the IS FoS . The FoS predictions from
261 the FE method decline steeply as the L/H ratio increases, so that the IS predictions are within 10% of
262 the FE prediction for L/H ratios greater than 10 and within 5 % for L/H ratios greater than 12. The
263 FE predictions asymptote at the IS FoS . We can use the difference between the FE and IS methods at
264 any given L/H ratio as an indicator of the error in the IS method resulting from the assumption of
265 infinite length. We can then use the length at which the IS method predictions fall within 5 or 10% of
266 the FE predictions to calculate a critical L/H ratio (L/H_{crit}) at which the assumption of infinite length
267 can be considered reasonable. However, we need to know how general this result is under the range
268 of plausible conditions and which other properties of the slope exert a controlling influence on
269 L/H_{crit} . The systematic parameter exploration provides the data required to address these questions
270 and can most easily be visualised by calculating the difference between IS and FE predictions across
271 the range of L/H ratios then normalising this difference as a percentage of the FE FoS . The resultant
272 curves are shown in Figure 4b for the unsaturated cases.

273

274 <Figure 4 near here>

275

276 During the systematic parameter exploration, cohesion appeared to exert the strongest control on the
277 *FoS* difference curves and on the L/H_{crit} value. In fact when cohesion was set to zero the FE
278 predictions did not fall outside 10% of the IS predictions even at the shortest L/H ratio (4).
279 Examining the deformed post failure mesh for cohesionless soils within the FE method revealed that
280 they fail in the top layer of elements (Figure 5a). This result fits closely with the IS method for
281 cohesionless soils, which assumes that failure is equally likely at all depths. In this case we would
282 expect failure at an infinitely shallow depth where the additional reinforcement at the toe would be
283 least, the length / depth ratio would be infinite and the infinite length assumption would be most
284 completely fulfilled. In the FE scheme, failure at an infinitely small depth would be represented as
285 failure in the top layer of elements (Figure 5a) but this makes the results difficult to interpret in terms
286 of critical L/H values since in this case L/H will always be infinite independent of the domain
287 dimensions and any departure from this will be a function of the discretisation of the domain. As a
288 result, we modified our sampling to sample three further cohesions: a negligible but non zero
289 cohesion (0.1 kPa); a very low cohesion (1 kPa) and a midpoint between the two previous cohesion
290 limits (10 kPa).

291

292 <Figure 5 near here>

293

294 Increasing cohesion slightly to 0.1 kPa forces the failure plane down below the first row of elements
295 (Figure 5b) but not always to the full depth of the model domain. In this situation the FE method
296 captures the competing effects of: additional downslope driving force with depth (represented in the
297 IS method); but also additional reinforcement with depth at the downslope margin of the landslide.
298 As a result, the FE model's failure plane depth differs from the IS prediction, which is always at the
299 base of the domain for cohesive soils. These FE model runs provide reliable L/H_{crit} predictions that
300 are often very small (Figure 4b), immediately suggesting that the L/H_{crit} value provided by Griffiths

1
2
3
4
5
6
7
8
9
10
11
12
13
14
15
16
17
18
19
20
21
22
23
24
25
26
27
28
29
30
31
32
33
34
35
36
37
38
39
40
41
42
43
44
45
46
47
48
49
50
51
52
53
54
55
56
57
58
59
60

301 *et al.* (2011) is only one example of a range of possible values and that varying slope properties leads
302 to different L/H_{crit} values.

303

304 Increasing the cohesion further to 1 kPa we find that the failure plane is now forced down to the base
305 of the model domain (Figure 5c). For these slope properties the curve is much steeper and more
306 similar to the results reported by Griffiths *et al.* (2011) (Figure 4b). Further increases in cohesion, to
307 10 kPa (a relatively high value for colluvial soils; see Hammond *et al.*, 1992), result in only small
308 changes to the form of the failure (Figure 5d) and to the L/H_{crit} value (Figure 4b). Figure 4b shows
309 the form of the *FoS* difference curves at the limits of the slope properties but is difficult to interpret
310 in terms of the influence of individual parameters on the L/H_{crit} value because: 1) it only shows
311 results for the extremes; and 2) the parameter combinations are difficult to differentiate. We address
312 these limitations using the random parameter exploration.

313

314 ***Random Parameter Exploration***

315 The results from the random parameter exploration are displayed as a series of scatter plots in Figure
316 6. The patterns for each parameter are similar for convergence at 5 and 10% thresholds but with a
317 lower maximum L/H_{crit} value for the 10% than the 5% threshold. They show that for almost all
318 parameter combinations the IS predictions converge to within 5 and 10% of those from the FE
319 method at L/H ratios of no more than 25 and 18 respectively.

320

321 <Figure 6 near here>

322

323 Of the six infinite slope parameters L/H_{crit} appears most sensitive to slope angle, with a strong
324 negative trend to the upper L/H_{crit} limit with slope. L/H_{crit} is also sensitive to, soil depth, normalised
325 free surface height and friction angle. There are strong negative trends to the upper L/H_{crit} limit for,
326 friction angle and soil depth and nonlinear negative trends to the lower L/H_{crit} limit for soil depth and
327 normalised free surface height so that low L/H_{crit} values are only possible for soils deeper than 1 m

328 and normalised free surface heights greater than 0.2. Increasing cohesion from very low values
329 causes a rapid nonlinear increase in the upper L/H_{crit} limit. The highest L/H_{crit} values are associated
330 with high cohesion; and low soil depth, slope angle and friction angle; the lowest L/H_{crit} values are
331 associated with low cohesion; and high soil depth, normalised free surface height and slope angle.

332

333 Discussion

334 *Critical length depth ratio*

335 Both the systematic and random parameter explorations confirm that the FoS predictions from the
336 FE method converge on those of the IS method across the full range of slope properties and
337 geometries that we might find in a catchment. The critical length depth ratio (L/H_{crit}) at which the FE
338 predictions converge to within 5 or 10% of the IS predictions varies with friction angle, cohesion,
339 soil depth, normalised free surface height and slope angle but is insensitive to soil unit weight. For a
340 5% threshold, L/H_{crit} values can range from 4 (effectively the detection limit for our study) to 25 and
341 for a 10% threshold they vary from 4 to 18.

342

343 Slope angle appears the dominant control on the upper limit to L/H_{crit} values. This is perhaps
344 unsurprising given that our definitions of length and depth are planimetric and vertical respectively.
345 As slope angle (β) increases the true length (L_t) increases relative to the planimetric length (L_p)
346 according to: $L_p = L_t / \cos(\beta)$ while the true (slope perpendicular) depth (H_t) decreases relative to the
347 vertical depth (H_v) according to: $H_t = H_v / \cos(\beta)$. As a result the true length depth ratio (L_t/H_t) is
348 related to the planimetric length depth ratio (L_p/H_v) according to $L_t/H_t = L_p/H_v (1/\cos^2(\beta))$. The
349 decrease in L/H_{crit} with slope angle closely follows the expected decrease resulting from this
350 difference between true and planimetric dimensions (grey lines in Figure 6). Despite this, we have
351 continued to use planimetric lengths and vertical depths since these are the dimensions commonly
352 used within catchment slope stability models. Much of the remaining variability is related to the
353 proportion of the soil strength made up by cohesion. We know from Figure 4 and Figure 5 that the
354 lowest L/H_{crit} values will always be found in cohesionless soils; and from Figure 6 that shallow soils

1
2
3
4
5
6
7
8
9
10
11
12
13
14
15
16
17
18
19
20
21
22
23
24
25
26
27
28
29
30
31
32
33
34
35
36
37
38
39
40
41
42
43
44
45
46
47
48
49
50
51
52
53
54
55
56
57
58
59
60

355 with high cohesion have higher L/H_{crit} values. However, even the steep ($>30^\circ$), shallow (<1 m), low
356 cohesion (<5 kPa) and high friction ($>30^\circ$) soils commonly found in upland catchments show a
357 relatively broad range of L/H_{crit} values (5-15 at 10% and 5-20 at 5%). With generalisation to all site
358 properties considered the infinite length assumption within the IS method results in errors of less
359 than 10% for L/H ratios greater than 18 and less than 5% for L/H ratios greater than 25 (Figure 6).
360 This has important implications for slope stability modelling using the infinite slope method and we
361 will explore these in detail in the following section.

362

363 ***Implications for geomorphic and landscape evolution models***

364 Catchment landslide models solve the infinite slope equation for each cell in a mesh. They assume
365 implicitly that the (downslope) length and (across slope) width of these cells represent the
366 dimensions of the predicted landslide (Dietrich *et al.*, 2008) and that these dimensions are large
367 enough relative to the failure plane that the infinite slope assumption is valid (Ray *et al.*, 2010). Our
368 results suggest that the infinite length assumption is valid, and results in less than 5% error for
369 landslides (and therefore model cells) with L/H ratios greater than 25 independent of material
370 properties. This validity will hold provided the grid resolution is more than 25 times the expected
371 failure plane depth. For example, many studies use a spatially constant failure plane depth of ~ 1 m
372 (e.g. Montgomery and Deitrich, 1994; Wu and Sidle, 1995). In this case, models with a grid
373 resolution of 25 m or more can apply the infinite slope method without significant length effects.
374 However, for models with a cell size less than 25 times the assumed landslide failure plane depth,
375 edge effects become possible and are likely to be significant if the length / depth ratio drops below 8.
376 In these cases many of the IS predictions differed from the FE predictions by greater than 50%.
377 Assuming failures of equal length and width, with a 1 m depth, this would mean that even groups of
378 ~ 60 1 m resolution cells are likely to be predicted as 50% less stable than they should be as a result
379 of length effects not represented by the infinite slope method. The dependence of the validity of the
380 infinite slope model upon cell size emphasises that care is required in assuming that higher
381 resolution topographic data always improve identification of landslide risk. Although the coarser cell

382 size may result in error because of the minimum landslide area that can be identified, higher
383 resolution data may result in error since the identified landslides may violate the infinite slope length
384 assumption.

385

386 To demonstrate the implications that this has for a catchment scale stability model we applied a
387 simple grid based stability model, using photogrammetrically derived topographic data (Milledge *et*
388 *al.*, 2009), to produce a set of predicted landslides for a 1 km² study area in the English Lake
389 District, Northern England (Warburton, *et al.* 2008). As we have discussed above, the main
390 difference in catchment scale stability models is the hydrological treatment used to define the pore
391 water pressure field. There is considerable debate around what drives the pore water pressure
392 increase that triggers landslides, with different groups arguing that it is: dominated by lateral
393 redistribution of water (e.g. Montgomery and Dietrich 1994; 2004; Montgomery *et al.*, 2002);
394 dominated by vertical infiltration (e.g. Iverson, 2000; 2004); or a combination of these (e.g.
395 D'Odorico and Fagherazzi, 2003). We will give an example for the simple and widely used case
396 where the pore water pressure field is driven by lateral redistribution. To do this we applied
397 SHALSTAB (Dietrich and Montgomery, 1998) in a deterministic sense (i.e. for a defined rainfall
398 and transmissivity). This model setup is analogous to the stability treatment within those landscape
399 evolution models that attempt to model hydrologically triggered landslides (e.g. Tucker and Bras,
400 1998). While it is very simple, its basis around the topographic control on spatial soil moisture is
401 very common (e.g. Wu and Sidle, 1995; Burton and Bathurst, 1998; Pack *et al.*, 1998; Borga *et al.*,
402 2002; Vanacker *et al.*, 2003; Dhakal and Sidle, 2004; Reid *et al.*, 2007; Simoni *et al.*, 2008; for
403 exceptions see: Iverson, 2000; Baum *et al.*, 2008).

404

405 We ran the model to predict landslides in two different scenarios: 1) the most common scenario,
406 using a coarse (10 m) grid resolution since this is a resolution typical of the most widely available
407 topographic data; and 2) the increasingly common scenario of finer (1 m) grid resolution to take
408 advantage of the constantly improving topographic data.

409

1
2
3
4
5
6
7
8
9
10
11
12
13
14
15
16
17
18
19
20
21
22
23
24
25
26
27
28
29
30
31
32
33
34
35
36
37
38
39
40
41
42
43
44
45
46
47
48
49
50
51
52
53
54
55
56
57
58
59
60

410 <Figure 7 near here>

411

412 Existing research has highlighted the influence of grid resolution on this type of model (e.g. Dietrich
413 and Montgomery, 1998; Claessens *et al.*, 2005). Our predicted landslides have characteristics that
414 are consistent with previous findings, particularly that new areas of potential instability are identified
415 at finer resolution (e.g. upper left corner of the Figure 7b). These relate to improved topographic
416 representation, which captures small steep areas that were previously smoothed out at the coarser
417 resolution. We also find that many of the predicted landslides are long for both the high and low
418 resolution model runs. The hydrological model generates patches of high pore water pressure that are
419 long in a downslope direction. As a result the model predicts long landslides and with high L/H
420 ratios that minimise the error associated with using the IS method. This suggests that the IS method
421 can applied in this case with high resolution data without violating its infinite length assumption. It is
422 worth noting that these long zones of predicted instability are a function of the model's assumption
423 that lateral redistribution drives pore water pressure patterns. It is the underlying hydrological
424 processes that drive characteristic L/H ratios; and these produce slides with L/H ratios that do not
425 violate the infinite slope stability assumption in this case. This suggests that the acceptability of the
426 IS model depends not only on data resolution but also on catchment hydrology and its representation
427 in the landslide model. Models with different hydrological representation might produce zones of
428 instability with different geometries, although lateral redistribution remains important control
429 through its influence on antecedent pore water pressures (Iverson, 2000; Montgomery and Dietrich,
430 2004). The suitability of these models will need to be assessed with reference to our findings on the
431 critical L/H ratio at which the IS method becomes applicable. Critically, our results do not give a
432 single answer on the suitability of the IS method for geomorphological slope stability modelling, but
433 they provide a tool to assess its suitability on a case by case basis, something that should be a routine
434 part of testing these models.

435

436 While finer grid resolutions still predict long landslides the predicted width is dramatically reduced.

437 This prompts an important question: how reasonable is the assumption of infinite width and what are

438 the critical width depth ratios at which the infinite slope assumptions break down? This question
439 cannot be addressed using the 2D finite element geotechnical model used in this study, since it also
440 assumes a slope of infinite width. Instead, solving this question would require a similar research
441 design within a 3D model, such models exist and research to address this question is underway.

442

443 **Conclusion**

444 Factor of safety predictions from the Finite Element method always converge to within 5 % of those
445 from the infinite slope method when the length / depth ratio exceeds 25. However, they can converge
446 at much lower length / depth ratios depending on the geometry and material properties of the slope.
447 The critical length depth ratio at which the predictions converge is in part controlled by the
448 proportion of the soil strength that comes from cohesion rather than from friction with the longer
449 length depth ratios required for more cohesive soils and very rapid convergence at low length depth
450 ratios for low cohesion soils.

451

452 The infinite length assumption within the infinite slope method is valid for many of the existing
453 modelling studies, which have used a coarse (>25 m) resolution. For models with a finer resolution
454 (<10 m) the assumption of infinite length might be less valid depending on the assumed landslide
455 failure plane depth and on the material properties. However, if lateral subsurface flow plays a role in
456 defining pore water pressure then its spatial organisation mitigates against predicting short landslides
457 and minimises the risk that predicted landslides will have length depth ratios less than 25.

458

459 In this case, whilst it is unlikely that the infinite length assumption introduces error into the stability
460 predictions because modelled landslides are often long, the infinite width assumption is more likely
461 to be violated since predicted landslides get narrower as the grid resolution is reduced. It may be
462 width and not length that limits the applicability of the infinite slope method and maintains the
463 stability of potential landslides. This is a topic that requires further research since it is not tractable
464 within a standard 2D geotechnical profile treatment but requires a 3D approach.

465

466 **Acknowledgements**

467 Data used as part of this research were funded by NERC Research Grant NE/D521481/1 to JW.

468 DGM was funded by NERC PhD Studentship NER/S/A/2004/12248 and NERC Fellowship

469 NE/H015949/1.

470

471 **References**

472 Bathurst JC, Moretti G, El-Hames A, Moaven-Hashemi A, Burton A. 2005. Scenario modelling of
473 basin-scale, shallow landslide sediment yield, Valsassina, Italian Southern Alps. *Natural Hazards
474 and Earth System Sciences* **5**: 189-202.

475 Baum RL, Savage WZ, Godt JW. 2008. TRIGRS - a fortran program for transient rainfall infiltration
476 and grid-based regional slope stability analysis, version 2.0. In, *Open File Report* (p. 81): U.S.
477 Geological Survey.

478 Borga M, Dalla Fontana G, Gregoretti C, Marchi L. 2002. Assessment of shallow landsliding by
479 using a physically based model of hillslope stability. *Hydrological Processes* **16**: 2833-2851.

480 Burton A, Bathurst JC. 1998. Physically based modelling of shallow landslide sediment yield at a
481 catchment scale. *Environmental Geology* **35**: 89-99.

482 Casadei M, Dietrich WE, Miller NL. 2003. Testing a model for predicting the timing and location of
483 shallow landslide initiation in soil-mantled landscapes. *Earth Surface Processes and Landforms* **28**:
484 925-950.

485 Chugh AK. 2003. On the boundary conditions in slope stability analysis. *International Journal for
486 Numerical and Analytical Methods in Geomechanics* **27**: 905-926.

487 Claessens L, Heuvelink GBM, Schoorl JM, Veldkamp A. 2005. DEM resolution effects on shallow
488 landslide hazard and soil redistribution modelling. *Earth Surface Processes and Landforms* **30(4)**:
489 461-477, doi: 10.1002/esp.1155

- 1 490 Crosta GB, Frattini P. 2003. Distributed modelling of shallow landslides triggered by intense
2 rainfall. *Nat. Hazards Earth Syst. Sci.* **3**: 81-93.
- 3
4 492 Dhakal AS, Sidle RC. 2004. Distributed simulations of landslides for different rainfall conditions.
5
6 493 *Hydrological Processes* **18**: 757-776.
- 7
8
9 494 Dietrich WE, McKean J, Bellugi D, Perron T. 2008. The prediction of shallow landslide location and
10 size using a multidimensional landslide analysis in a digital terrain model. In *Fourth International*
11
12 495 *Conference on Debris-Flow Hazards Mitigation: Mechanics, Prediction, and Assessment (DFHM-*
13
14 496 *4), Chengdu, China, September 10-13, 2007*, Chen CL, Major JJ (eds). Amsterdam: IOS Press.
- 15
16 497
17
18 498 Dietrich WE, Montgomery DR. 1998. SHALSTAB: a digital terrain model for mapping shallow
19 landslide potential. In, *Technical Report* (p. 29): NCASI.
- 20
21
22 500 D'Odorico P, Fagherazzi S. 2003. A probabilistic model of rainfall-triggered shallow landslides in
23 hollows: A long-term analysis, *Water Resources Research.* **39**: 1262, doi:10.1029/2002WR001595.
- 24
25 501
26
27 502 Gabet EJ, Dunne T. 2002. Landslides on coastal sage-scrub and grassland hillslopes in a severe El
28 Nino winter: The effects of vegetation conversion on sediment delivery. *Geological Society of*
29
30 503 *America Bulletin* **114**: 983-990.
- 31
32
33 504
34 505 Griffiths DV. 1982. Computation of bearing capacity factors using finite elements. *Geotechnique*
35
36 506 **32(3)**: 195-202.
- 37
38 507 Griffiths DV, Huang JS, Dewolfe GF. 2011. Numerical and analytical observations on long and
39 infinite slopes. *International Journal for Numerical and Analytical Methods in Geomechanics* **35**:
40
41 508 569-585.
- 42
43
44 510 Griffiths DV, Lane PA. 1999. Slope stability analysis by finite elements. *Geotechnique* **49**: 387-403.
- 45
46 511 Griffiths DV, Marquez RM. 2007. Three-dimensional slope stability analysis by elasto-plastic finite
47 elements. *Geotechnique* **57**: 537-546.
- 48
49
50
51 513 Haefeli R. 1948. The stability of slopes acted upon by parallel seepage. In *International Conference*
52
53 514 *on Soil Mechanics and Foundation Engineering*; 57-62.
- 54
55
56 515 Hammah RE, Yacoub TE, Corkum B, Curran JH. 2005. A comparison of finite element slope
57 stability analysis with conventional limit-equilibrium investigation. In *58th Canadian Geotechnical*
58
59 516
60

- 1
2
3
4
5
6
7
8
9
10
11
12
13
14
15
16
17
18
19
20
21
22
23
24
25
26
27
28
29
30
31
32
33
34
35
36
37
38
39
40
41
42
43
44
45
46
47
48
49
50
51
52
53
54
55
56
57
58
59
60
- 517 and 6th Joint IAH-CNC and CGS Groundwater Specialty Conferences - GeoSask 2005. Saskatoon;
518 480-487.
- 519 Haneberg WC. 2004. A rational probabilistic method for spatially distributed landslide hazard
520 assessment. *Environmental & Engineering Geoscience* **10**: 27-43.
- 521 Iverson RM. 2000. Landslide triggering by rain infiltration. *Water Resources Research* **36**: 1897-
522 1910.
- 523 Iverson RM. 2004. Comment on “Piezometric response in shallow bedrock at CB1: Implications for
524 runoff generation and landsliding” by David R. Montgomery, William E. Dietrich, and John T.
525 Heffner, *Water Resources Research* **40**: W03801, doi:10.1029/2003WR002077.
- 526 Larsen IJ, Montgomery DR, Korup O. 2010. Landslide erosion controlled by hillslope material.
527 *Nature Geosci* **3**: 247-251.
- 528 Milledge DG. 2009. Digital filtering of generic topographic data in geomorphological research.
529 *Earth Surface Processes and Landforms* **34**: 63-74.
- 530 Montgomery DR, Dietrich WE. 1994. A Physically-Based Model for the Topographic Control on
531 Shallow Landsliding. *Water Resources Research* **30**: 1153-1171.
- 532 Montgomery DR, Dietrich WE, Heffner JT. 2002. Piezometric response in shallow bedrock at CB1:
533 Implications for runoff generation and landsliding, *Water Resources Research*. **38**(12): 1274,
534 doi:10.1029/ 2002WR001429.
- 535 Montgomery DR, Dietrich WE. 2004. Reply to comment by Richard M. Iverson on “Piezometric
536 response in shallow bedrock at CB1: Implications for runoff generation and landsliding,” *Water*
537 *Resources Research* **40**: W03802, doi:10.1029/2003WR002815.
- 538 Pack RT, Tarboton DG, Goodwin CN. 1998. The SINMAP approach to terrain stability mapping In,
539 *8th International Congress of the International Association for Engineering Geology and the*
540 *Environment*. Vancouver, Canada.
- 541 Perzyna P. 1966. Fundamental problems in viscoplasticity. *Advances in Applied Mechanics* **9**: 243–
542 377.

- 1 543 Ray RL, Jacobs JM, de Alba P. 2010. Impacts of Unsaturated Zone Soil Moisture and Groundwater
2 544 Table on Slope Instability. *Journal of Geotechnical and Geoenvironmental Engineering* **136**: 1448-
3 545 1458.
4
5
6 546 Reid SC, Lane SN, Montgomery DR, Brookes CJ. 2007. Does hydrological connectivity improve
7
8 547 modelling of coarse sediment delivery in upland environments? *Geomorphology* **90**: 263-282.
9
10 548 Simoni S, Zanotti G, Bertoldi G, Rigon R. 2008. Modelling the probability of occurrence of shallow
11
12 549 landslides and channelized debris flows using GEOtop-FS. *Hydrological Processes* **22**: 2248-2263.
13
14 550 Skempton AW, DeLory FA. 1957. Stability of natural slopes in London clay. In *4th International*
15
16 551 *Conference on Soil Mechanics and Foundation Engineering*; 378-381.
17
18 552 Taylor DW. 1948. *Fundamentals of Soil Mechanics*. Wiley: New York.
19
20 553 Tucker GE, Bras RL. 1998. Hillslope processes, drainage density, and landscape morphology. *Water*
21
22 554 *Resources Research* **34**: 2751-2764.
23
24 555 Vanacker V, Vanderschaeghe M, Govers G, Willems E, Poesen J, Deckers J, De Bievre B. 2003.
25
26 556 Linking hydrological, infinite slope stability and land-use change models through GIS for assessing
27
28 557 the impact of deforestation on slope stability in high Andean watersheds *Geomorphology* **52**: 299-
29
30 558 315.
31
32 559 Warburton J, Milledge DG, Johnson RM. 2008. Assessment of shallow landslide activity following
33
34 560 the January 2005 storm, Northern Cumbria. *Proceedings of the Cumberland Geological Society* **7**:
35
36 561 263-283.
37
38 562 Wu WM, Sidle RC. 1995. A Distributed Slope Stability Model for Steep Forested Basins. *Water*
39
40 563 *Resources Research* **31**: 2097-2110.
41
42 564 Zienkiewicz OC, Humpheson C, Lewis RW. 1975. Associated and Non-Associated Visco-Plasticity
43
44 565 and Plasticity in Soil Mechanics. *Geotechnique* **25**: 671-689.
45
46
47
48
49
50
51 566
52
53
54
55
56
57
58
59
60

1
2
3
4
5
6
7
8
9
10
11
12
13
14
15
16
17
18
19
20
21
22
23
24
25
26
27
28
29
30
31
32
33
34
35
36
37
38
39
40
41
42
43
44
45
46
47
48
49
50
51
52
53
54
55
56
57
58
59
60

567 Tables

568 **Table 1: Parameters varied within the parameter exploration with the range over which they were**
569 **varied. Young's Modulus and Poisson's Ratio were held constant at the values below.**

Parameter	Value Range
Friction Angle (ϕ')	15 - 45°
Cohesion (c')	0 - 20 kPa
Soil Depth (H)	0 - 3 m
Normalised free surface height (m)	0 - 1
Soil Unit Weight (γ_{sat})	1.1 - 1.8 kN m ⁻³
Slope Angle (β)	15 - 45°
Young's Modulus	10 ⁵ kPa
Poisson's Ratio	0.3

570

571 Figures

572 **Figure 1: Cumulative probability distributions for the length / depth ratios of landslides from two**
573 **inventories in Cumbria, UK (Warburton *et al.*, 2008) and and California, USA (Gabet and Dunne, 2003).**

574

575 **Figure 2: Schematic profile view through an infinite slope showing the relevant forces and lengths.**

576

577 **Figure 3: example finite element mesh of 8-node quadrilateral elements annotated to show the**
578 **relevant lengths and angles used within the model.**

579

580 **Figure 4: A) relationship between length / depth ratio and factor of safety for infinite slope (IS) and**
581 **finite element (FE) models for an example slope with $\phi'=30^\circ$, $c'=20$ kPa, $\gamma_{sat}=19$ kN m³, $H=5$ m and**
582 **$\beta=25^\circ$; B) difference between FE and IS predictions (expressed as a percentage of FE FoS) for**
583 **different length / depth ratios.**

584

585 **Figure 5: deformed meshes showing the shape of the failure mechanism for a slope with $\phi'=20^\circ$,**
586 **$\gamma_{sat}=1.9$ kN m⁻³, $m=0$, $L=2$ m, $H=0.5$ m, $\beta=20^\circ$ and cohesions of: A) 0 kPa, B) 0.1 kPa, C) 1 kPa, and**
587 **D) 10 kPa. Displacements are exaggerated for visualisation and should be interpreted as relative**
588 **rather than absolute.**

589

590 **Figure 6: uncertainty plots showing variation in the length / depth ratio at which the infinite slope**
591 **predictions converge to within 5 and 10% of the finite element predictions (L/H_{crit}) for a range of:**
592 **friction angles, soil cohesions, soil depths, normalised free surface heights, soil unit weights and**
593 **slope angles. The bottom row shows results for parameters sampled to zero in semi-logarithmic**
594 **space to illustrate their influence at low values. The grey lines on the slope angle plots have the**
595 **equation $y = a \cos^2(\beta)$, where $a = 24$ and 16 for the upper and lower plots respectively.**

596

597 **Figure 7: predicted landslides from a 1 km² patch of a grid based stability model with $\phi'=40^\circ$, $c'=1$ kPa,**
598 **$\gamma_{sat}=1.7$ kN m⁻³, transmissivity = 0.01 mm h⁻¹ and steady state rainfall rate = 100 mm h⁻¹, $H = 1$ m,**
599 **cellsize is 10 m for a and 1 m for b.**

600

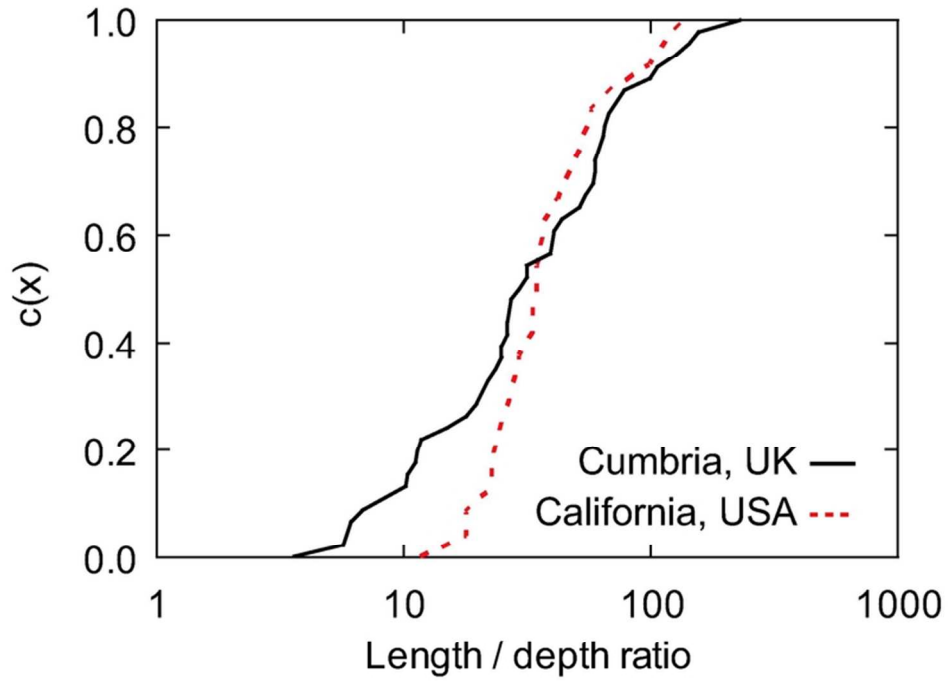


Figure 1: Cumulative probability distributions for the length / depth ratios of landslides from two inventories in Cumbria, UK (Warburton et al., 2008) and and California, USA (Gabet and Dunne, 2003).
71x55mm (300 x 300 DPI)

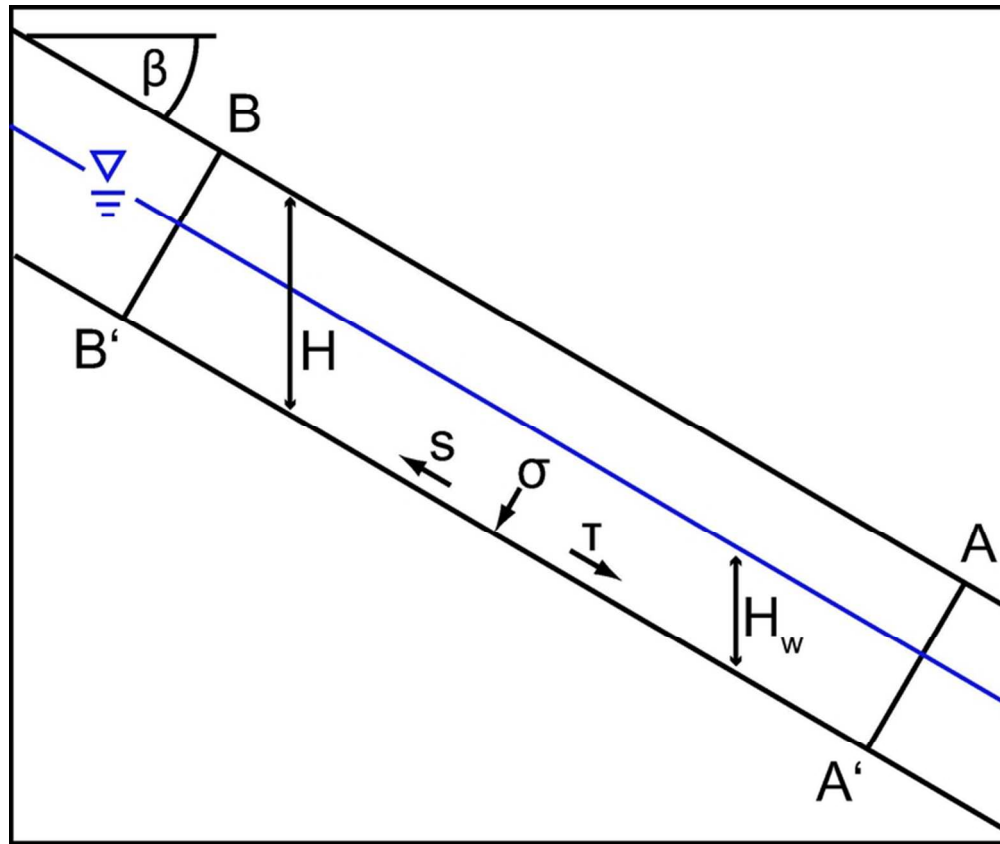


Figure 2: Schematic profile view through an infinite slope showing the relevant forces and lengths.
65x55mm (300 x 300 DPI)

1
2
3
4
5
6
7
8
9
10
11
12
13
14
15
16
17
18
19
20
21
22
23
24
25
26
27
28
29
30
31
32
33
34
35
36
37
38
39
40
41
42
43
44
45
46
47
48
49
50
51
52
53
54
55
56
57
58
59
60

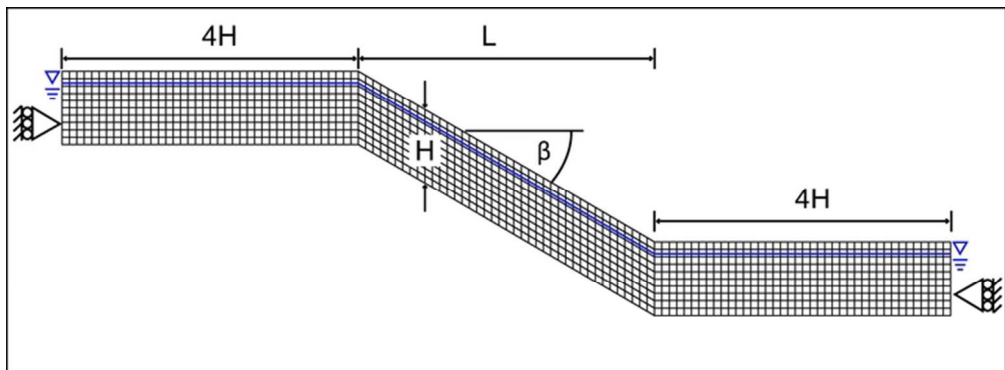


Figure 3: example finite element mesh of 8-node quadrilateral elements annotated to show the relevant lengths and angles used within the model.
65x24mm (300 x 300 DPI)

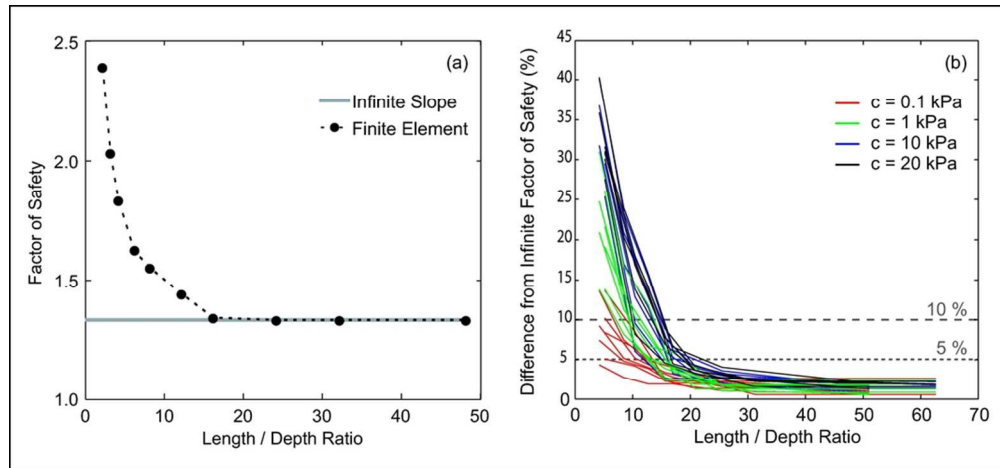


Figure 4: A) relationship between length / depth ratio and factor of safety for infinite slope (IS) and finite element (FE) models for an example slope with $\phi'=30^\circ$, $c'=20$ kPa, $\gamma_{sat}=19$ kN m³, $H=5$ m and $\beta=25^\circ$; B) difference between FE and IS predictions (expressed as a percentage of FE FoS) for different length / depth ratios.
 90x42mm (300 x 300 DPI)

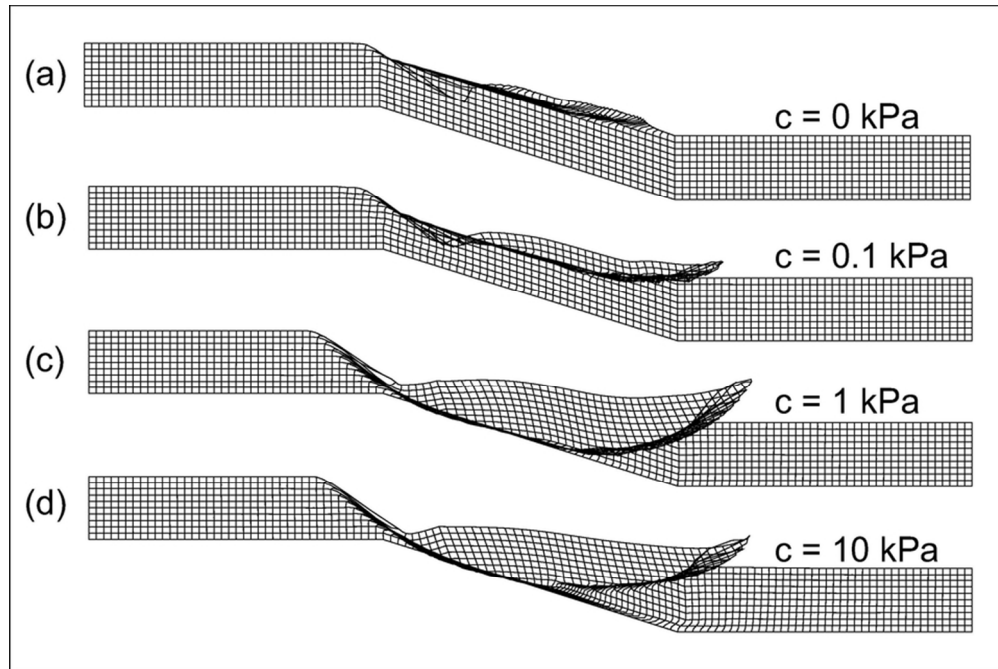


Figure 5: deformed meshes showing the shape of the failure mechanism for a slope with $\phi' = 20^\circ$, $\gamma_{\text{sat}} = 1.9 \text{ kN m}^{-3}$, $m = 0$, $L = 2 \text{ m}$, $H = 0.5 \text{ m}$, $\beta = 20^\circ$ and cohesions of: A) 0 kPa, B) 0.1 kPa, C) 1 kPa, and D) 10 kPa. Displacements are exaggerated for visualisation and should be interpreted as relative rather than absolute.

81x54mm (300 x 300 DPI)

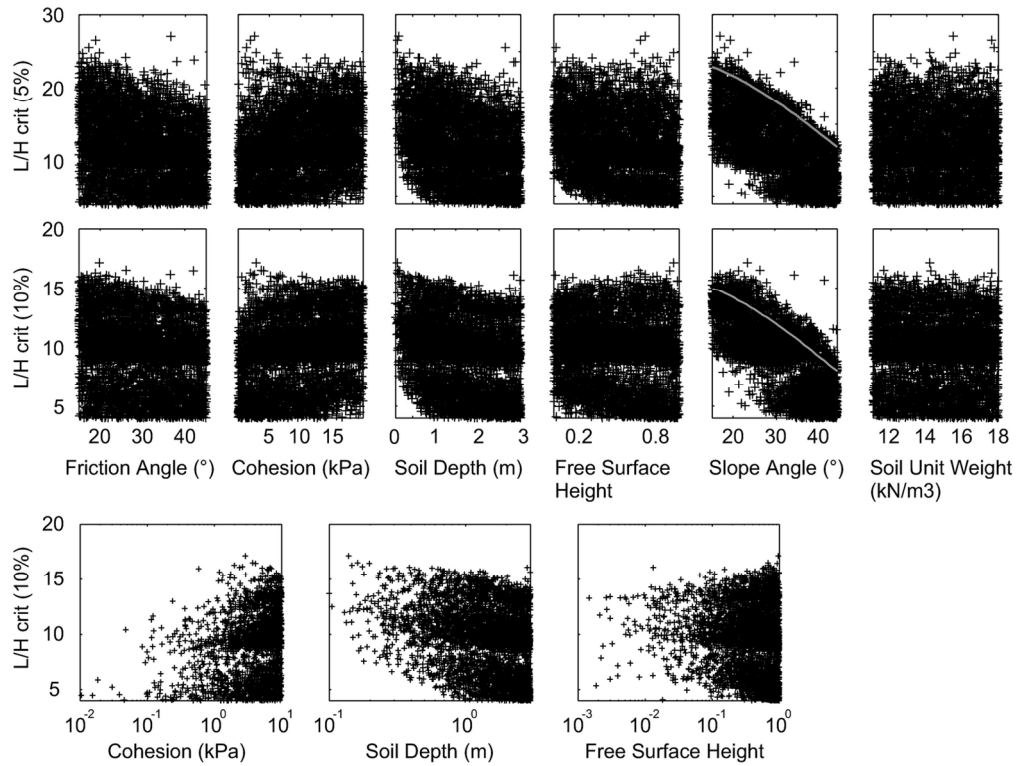


Figure 6: uncertainty plots showing variation in the length / depth ratio at which the infinite slope predictions converge to within 5 and 10% of the finite element predictions (L/H_{crit}) for a range of: friction angles, soil cohesions, soil depths, normalised free surface heights, soil unit weights and slope angles. The bottom row shows results for parameters sampled to zero in semi-logarithmic space to illustrate their influence at low values. The grey lines on the slope angle plots have the equation $y = a \cos^2(\beta)$, where $a = 24$ and 16 for the upper and lower plots respectively.

133x101mm (300 x 300 DPI)

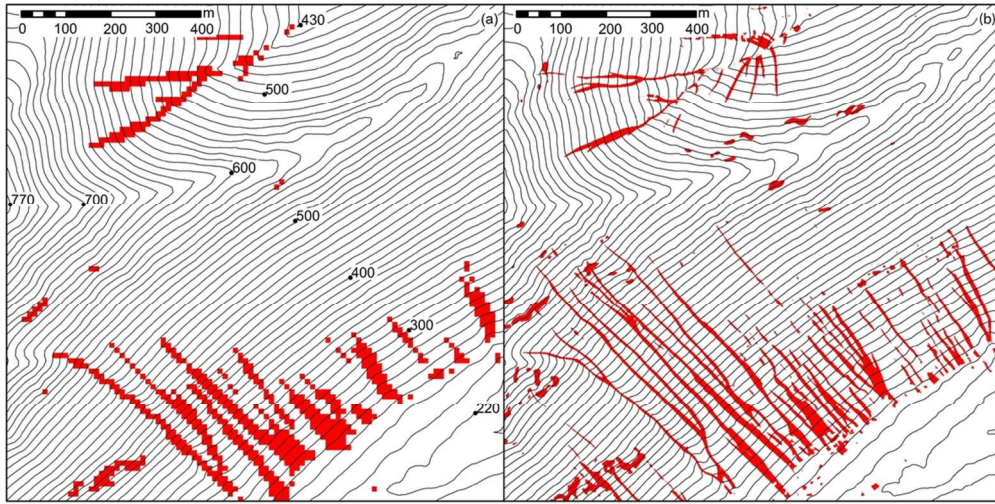


Figure 7: predicted landslides from a 1 km² patch of a grid based stability model with $\phi'=40^\circ$, $c'=1$ kPa, $\gamma_{sat}=1.7$ kN m⁻³, transmissivity = 0.01 mm h⁻¹ and steady state rainfall rate = 100 mm h⁻¹, $H = 1$ m, cellsize is 10 m for a and 1 m for b. 100x50mm (300 x 300 DPI)

1
2
3
4
5
6
7
8
9
10
11
12
13
14
15
16
17
18
19
20
21
22
23
24
25
26
27
28
29
30
31
32
33
34
35
36
37
38
39
40
41
42
43
44
45
46
47
48
49
50
51
52
53
54
55
56
57
58
59
60